

Dynamical pulse shaping in a nonlinear resonator

G. Steinmeyer, A. Buchholz, M. Hänsel, M. Heuer, A. Schwache, and F. Mitschke *
Institut für Quantenoptik, Universität Hannover, Welfengarten 1, 30167 Hannover, Germany
 (Received 13 October 1994)

A synchronously pumped passive ring resonator, containing an optical fiber as a nonlinear element, is studied experimentally and numerically. Period doubling cascades up to period 32 and chaos are observed in the sequence of pulse energies emerging from the resonator. We provide evidence that beyond this instability, individual pulses encounter an instability of their temporal profile. Pulse shapes develop a substructure that may be stationary, periodic, or chaotic. The full problem thus actually involves formation of a spatiotemporal structure. In contrast to many other spatiotemporal instabilities studied in optics, we deal here with strictly one-dimensional, longitudinal spatial structure.

PACS number(s): 42.50.Ne, 42.65.Re, 42.50.Rh

I. INTRODUCTION

Consider an optical resonator, filled with a material that has a nonlinear index of refraction. Ikeda and co-workers [1] have pointed out that such a system can display chaos if light above a certain threshold power is irradiated. The explanation relies on the interference between two waves: the input light, plus the light that has completed a round trip in the resonator, where the latter has undergone nonlinear interaction. This reasoning leads to the formulation of a simple recursive relation ("Ikeda map") which can be written as

$$A_n = A_{in} + \eta \exp \left[i \left(\varphi_0 + \frac{2\pi n_2 L}{\lambda} |A_{n-1}|^2 \right) \right] A_{n-1} . \quad (1)$$

Here, A_n denotes the electric field amplitude in the cavity after the n th round trip, A_0 the input field, η the feedback efficiency, φ_0 the static resonator phase, L the length of the Kerr medium, λ the wavelength, and n_2 the nonlinear index of refraction. Note that the equation in this simple form implies an instantaneous nonlinear response.

In a first experimental test of that theory, Nakatsuka *et al.* [2] used a single mode optical fiber as a nonlinear medium. Fibers have a very fast Kerr nonlinearity [3] that can be considered instantaneous for most purposes. Also, a suitably chosen fiber will guarantee a single transverse mode; complications from a possible generation of transverse beam structure (see, e.g., [4]), not considered in Eq. (1), are thus ruled out.

The disadvantage of fiber is that the nonlinear index change is small: For typical fibers, it is in the range of $3 \times 10^{-20} I$, where I is the intensity in the fiber (in W/m^2) [3]. This small value necessitates high light powers for

any appreciable effect, not easily attainable in cw operation. Therefore, a train of picosecond pulses from a mode locked laser was used in [2]. The round trip time of the cavity was matched to the pulse repetition time to ensure interference of each pulse with its counterpart from the previous round trip.

With this synchronously driven passive cavity, an instability was indeed observed in [2]. That work has therefore been considered a confirmation of Ikeda's prediction as well as the first demonstration of chaos in a passive optical system.

However, the laser was not only mode locked but also Q switched. Consequently, there were no steady conditions, and only transient behavior could be observed. Also, that experiment had no control over the crucial parameter of the cavity round trip phase. Therefore, no further analysis of the results was possible.

Several subsequent experimental approaches to the fiber ring system have been reported [5-7] that employed continuous trains of pulses from mode-locked pump lasers to assure steady conditions, but only [6] had control over the cavity phase. Meanwhile, considerable progress has been made in the understanding of the mechanism. In particular, the roles of modulational instability [7,8] and group velocity dispersion [6,9] were discussed. We basically corroborate the conclusions of these references. Beyond that, we present particularly clean experimental information on the temporal evolution. We do have knowledge of the cavity phase, and we are able to record long strings of data with the help of fast digitizing oscilloscopes. (First results from our experiment were given in [10,11].) On these data we base a detailed comparison with numerical calculations.

The approach with a one-dimensional mapping like Eq. (1) implies that each pulse is uniquely described by a single number, referring to its energy. However, for the plane wave case originally discussed by Ikeda [1], it has been shown in [12] that the fixed points of the Ikeda map are unstable to transverse spatial perturbations. Vallée [9] argued that in the case of transverse confinement by a waveguide, as considered here, an analogous argument

*Present address: Institut für Angewandte Physik, Correnstrasse 2/4, 48149 Münster, Germany.

should hold for the longitudinal spatial direction. As a consequence spatial structure should be inevitable, and a large number of degrees of freedom may be present. Thus, a one-dimensional mapping would have to fail. Van der Mark *et al.* [6] have presented experimental indications in support of this reasoning.

We show here in unprecedented clarity what other authors have argued before: a simple one-dimensional (1D) model like Eq. (1) is absolutely inadequate to describe the physics of a synchronously driven nonlinear ring resonator. We will demonstrate that structures form in the pulse shapes, which may be either stationary, or dynamically evolving. Thus, for any given pulse energy there can be a multitude of pulse shapes. These “longitudinal structures” indeed correspond to structures observed in a variety of optical experiments in the plane transverse to the propagation direction.

We will further show that group velocity dispersion in the resonator is a key parameter in this formation of structure. Experimental results and extensive numerical calculations will reveal its influence, and give an indication of the full complexity at work in this deceptively simple experimental situation.

II. THE ROLE OF DISPERSION

Group velocity dispersion, disregarded in some of the early studies, emerges now as one of the crucial ingredients [9]. The action of dispersion can be described as follows: Think of the pulses as being made up of many temporal “slices,” each of which occupies an infinitesimally narrow time slot. Now assume the absence of dispersion, and also exact synchronism of the resonator round trip time with the input pulse repetition time. Then, each slice will interact only with the corresponding slice in the following pulse, but not at all with neighboring slices. Consequently, the slices will evolve in total independence. If some of these slices then exhibit chaotic dynamics, we are faced with the paradox that infinitesimally close slices will exhibit macroscopically different behavior, which would produce an infinitely wide optical spectrum. It is obvious that the inclusion of dispersion removes this paradox because it creates an interaction between neighboring slices. The stronger the dispersion, the more correlated the temporal evolution of neighboring time slots. In this sense, dispersion is one of the most relevant parameters in the experiment. Other groups, insofar as they recorded time series from the experiment, were restricted to conditions of strong group velocity dispersion (silica fiber in the visible).

In order to vary dispersion, we selected fibers with staggered amounts of dispersion. In the case with lowest dispersion we approach the “paradox” case discussed above. In that case, total dispersion is dominated by higher order contributions, and the mechanism of coupling between the temporal slices is quite different. This will become apparent below.

III. EXPERIMENTAL SETUP AND PROCEDURES

The setup of our experiment is shown in Fig. 1. As a light source we employ an additive pulse mode-locked Nd:YAG (neodymium-doped yttrium aluminum garnet) laser at $\lambda = 1.3188 \mu\text{m}$ [13]. This laser produces a continuous train of pulses with a repetition rate of 82.4 MHz that are ≈ 12 ps wide, practically free of chirp, and sech^2 shaped. Average output powers up to 1.5 W and peak powers exceeding 1 kW are achieved so that nonlinear phase shifts of the order of π can be produced in just a few meters of fiber. Back reflections from the experiment into the laser are suppressed by an optical isolator. A half-wave retarder, together with the first polarizer in the isolator, serves as a variable attenuator to set the input optical power for the nonlinear resonator. Part of the laser beam is split off and sent into a fast photodiode so that the laser source is permanently monitored throughout our experiments. None of the instabilities described below occurs at this position.

The light enters the ring resonator through an input coupling mirror. It has a reflectivity of $R = 30\%$. GRIN lenses are employed for free space-to-fiber coupling; efficiencies of 60% are obtained. With all losses, the resonator has a finesse of 3.5.

Given the available optical power, there is a minimum value for the fiber length, dictated by the required nonlinear phase shifts. We use $L = 9.25$ m of fiber throughout. Additional air paths bring the effective resonator path length to 14.56 m. To achieve synchronous pumping, this total cavity length is fine-tuned with a delay line, so that the free spectral range ($f_0 = 20.6$ MHz) equals one-quarter of the pulse repetition rate ($f_r = 82.4$ MHz) to within a few tens of micrometers. The length of the cavity is adjusted for minimum threshold of the first bifurcation. This adjustment procedure provides a reproducibility of the cavity length better than $50 \mu\text{m}$.

Note that at any given time, there are in fact four

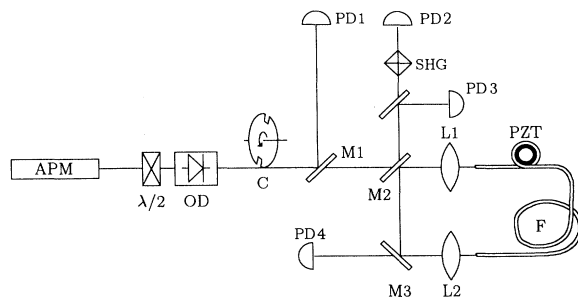


FIG. 1. Experimental setup. APM, additive pulse mode-locked Nd:YAG laser; $\lambda/2$, half wave retarder; OD, optical diode (Faraday rotator and polarizers); C, custom-made chopper wheel (see text); PZT, piezoelectric ring transducer; F, 9.1-m polarization-maintaining fiber; M_i , mirrors (M_1 has 4%, M_2 has 31%, and M_3 has 99% reflectivity); L_i , lenses; PD_i , photodiodes (PD_1 monitors the laser, PD_2 the frequency-doubled resonator output, PD_3 the resonator output, and P_4 the resonator phase); SHG, second harmonic generating crystal.

pulses traveling the fiber. However, their interaction is negligible, and in the subsequent analysis of the data, we will simply use only every fourth detector pulse. (In fact, comparisons of the four interleaved data streams provide some useful consistency checks.)

All fibers were single mode and polarization maintaining, and light was linearly polarized along the slow axis of the fiber throughout. Fiber ends were angle cut to reduce spurious reflections. According to earlier experience, manufacturer's information on fiber dispersion is not always very accurate. We therefore selected the fibers used here from the stock of one manufacturer (Fibercore, Chandlers Ford, U.K.) on the basis of our own measurements, using white light interferometry over a wavelength range from 1200 to 1750 nm in a setup similar to [14]. Table I lists the dispersion properties of all three fibers used here. The accuracy of these measurements was obviously most critical for fiber A. The reproducibility of its zero dispersion wavelength was ± 1 nm. The largest systematic errors are to be expected from the wavelength readout of the monochromator involved; we therefore calibrated this readout with the 1318.8 nm line of the Nd:YAG laser.

For a comparison with theory, we also determined the nonlinearity coefficient $\gamma = 2\pi n_2/\lambda A_{\text{eff}}$ of the fibers. A_{eff} is the effective mode field area of the fiber. This was done through comparison of directly measured self-phase modulated spectra and numerical results at different input powers similar to the method of [15]. Fiber parameters are given in Table I.

Thermal fluctuations and acoustic perturbations produce slight length changes that let the cavity phase drift over several free spectral ranges on slow time scales (milliseconds to seconds). This drift makes it impossible to take data at a known resonator phase unless either the resonator length is stabilized by some means, or the phase is somehow recorded along with all measurements. We use a fairly simple method that was already described in [10]. A custom-made chopper wheel is employed to repetitively switch between small signal and large signal regimes. At the same time, the resonator length is slowly ramped with a piezoelectric ring transducer (PZT). A 1% tap on the ring resonator is used to monitor the Airy function in the small signal case, so that the resonator phase during the relatively short large signal intervals can be interpolated.

At the remaining part of the input coupling mirror, we can monitor the processes in the ring with various techniques. All experimental results described below are taken at this output. One of the first checks was with a monochromator at the appropriate wavelengths to convince ourselves that there was no noticeable stimulated

Raman scattering.

In this paper we restrict ourselves to results based on direct digitalization of the pulses. Since the optical pulses are much faster than the temporal resolution of any electronics, we can only measure integrated values of pulse energies. Of course, any dynamical processes in the "central slice," i.e., at the pulse peak, will be nearly swamped in this integral value by contributions from the pulse wings. To discriminate the pulse peak against the wings, we send the resonator output light through a nonlinear optical crystal (LiIO_3) for second harmonic generation (SHG). The resulting red light is recorded with a Si avalanche diode-low noise amplifier combination with 300 MHz bandwidth (Analog Modules 713A-4-B). Its output is sent to a digital storage oscilloscope, the sampling rate of which is synchronized to the pulse repetition rate. At different stages of this research, either a Tektronix RTD710A or a LeCroy 9354L digital storage oscilloscope was used. Data are taken with 10-bit (Tektronix) or 8-bit (LeCroy) vertical resolution.

IV. EXPERIMENTAL RESULTS

A typical example for measured time series from fiber B (intermediate dispersion) is shown in Fig. 2. This example is compiled from 32 000 data points (pulse energies E_{SHG} at PD2) sampled every 48 ns. The trace covers a total time interval of 1.5 ms. Over this time interval, the resonator phase φ_0 is slowly ramped from 0.3π to -1.1π . From $\varphi_0 = 0$ to -0.3π we observe P2 behavior; modulation in the corresponding fundamental signal reaches a maximum depth of about 40%. From $\varphi_0 = -0.3\pi$ to $\varphi_0 = -0.6\pi$ there is a forward period-doubling cascade, which can be followed up to period 16. In the consecutive phase range, pulse energies form two broadbands, which finally merge to a single band like the one at the beginning of the time series. Similarly, there is a transition from irregular to periodic behavior at $\varphi_0 = 0.1\pi$ through reverse period-doubling bifurcations. We interpret the broadband structures as deterministic chaos.

Note that if the scan direction is reversed, transition points between periodic and chaotic behavior occur at slightly different positions. Moreover, we find differences in the dynamical behavior of the four pulses evolving in parallel in the resonator. In some cases we observe that one of the four interleaved time series shows, e.g., stable P1 behavior, while the others exhibit a P2. In other words, different dynamical patterns are possible for the same set of parameters, and there is hysteresis at the transition points.

A closer look at the time series reveals that at the bifurcation points there are several crossovers in the traces

TABLE I. Relevant properties of fibers used here. Dispersion values and nonlinearity refer to the laser wavelength $\lambda = 1318.8$ nm and to the slow axis of the fiber. All fibers were supplied by Fibercore.

Fiber	Type	λ_0 (nm)	β_2 (ps^2/km)	β_3 (ps^3/km)	γ ($\text{m}^{-1} \text{W}^{-1}$)
A	HB1500 (YD355-01)	1322	0.25	-0.08	4.7×10^{-3}
B	HB1250 (YD762-01C)	1420	7.4	-0.075	4.8×10^{-3}
C	HB1500 (YD535-01A)	1480	11.8	-0.064	8.0×10^{-3}

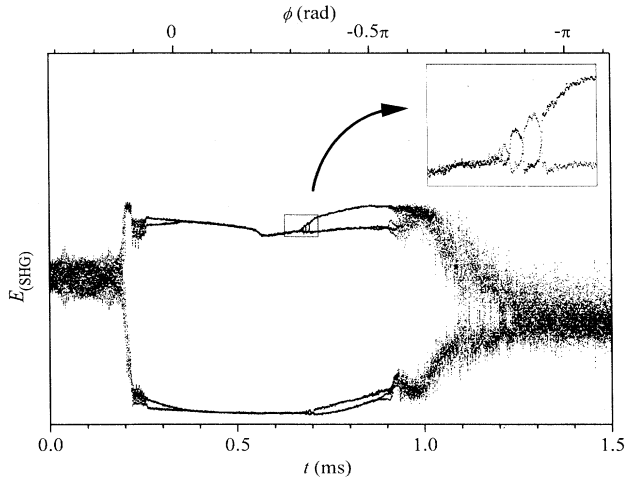


FIG. 2. Experimental recording of a time series. Data were sampled every 48 ns using SHG detection (PD2 in Fig. 1). The detector was ac coupled. To cover the interval of 1.5 ms a total number of 32 000 data points was recorded while the phase was slowly ramped. Peak power in the fiber was set to $P = 140$ W; this leads to a nonlinear phase shift of $\varphi_{nl} = 2\pi$. Dispersion: $\beta_2 = 7.4$ ps²/km, $\beta_3 = -0.075$ ps³/km. In the inset a magnification of a “wiggly” bifurcation is displayed.

(see inset). These “wiggly” bifurcations have been repeatedly observed in the periodic regime. They are most conspicuous in the case of the low dispersion fiber A. An explanation will be given below.

Figure 3 shows power spectra, calculated via Fourier transform of short segments (2048 to 8192 data points) of experimental time series. Subharmonic behavior of frequency f_0/x (period x) is denoted as Px . We routinely observe the period doubling sequence up to P16, and occasionally see P32. Note that it is generally hard to observe period doubling beyond P8 in optical systems. It is possible in our case because at the high frequencies involved here the signal is not corrupted by $1/f$ noise. We thus achieve a remarkable signal-to-noise ratio in the experiment.

The last two panels of Fig. 3 show a broadband background that corresponds to the chaotic bands in the time series. On top of this background there can be more (P2- χ) or less (χ) indication of periodic content. The partly chaotic, partly periodic signal could be either weak chaos or chaos in the pulse peak superimposed with P2 oscillation in the pulse wings. The ambiguity is resolved with the help of simultaneously recorded time series from both fundamental and second-harmonic generation and SHG (see Fig. 4), since the latter gives more weight to the peak and less to the wings. In comparison, there is a relative attenuation of the P2 feature in the second harmonic signal. We therefore conclude that in fact different segments of the pulses undergo different dynamics: the pulse peaks evolve chaotically while there is P2 behavior in the wings. This conclusion should already caution us that any characterization of the pulses by a single number each (its energy) is unlikely to capture the processes at work.

While the spectra display spectral information, we pro-

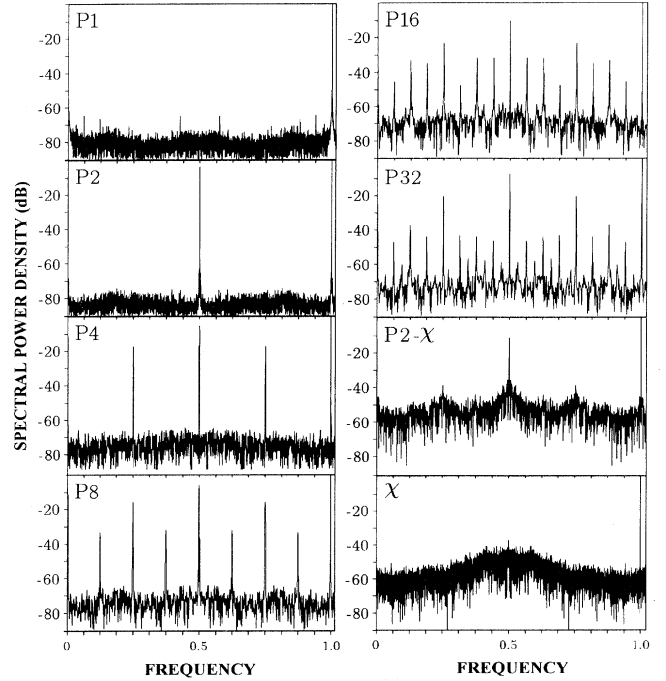


FIG. 3. Power spectra of experimental data. Frequencies are normalized to the repetition rate of $f_0=20.6$ MHz; subharmonic behavior of frequency f_0/x (period x) is denoted as Px . χ denotes a chaotic signal, and P2- χ a similar signal with a strong P2 component. Nonlinear and static resonator phases: (P1) $\varphi_{nl} = \pi$, $\varphi_0 = 0.2\pi$; (P2) $\varphi_{nl} = 1.5\pi$, $\varphi_0 = 0.3\pi$; (P4) $\varphi_{nl} = 1.5\pi$, $\varphi_0 = -0.3\pi$; (P8) $\varphi_{nl} = 1.7\pi$, $\varphi_0 = 0.1\pi$; (P16) $\varphi_{nl} = 2.4\pi$, $\varphi_0 = 0.1\pi$; (P32) $\varphi_{nl} = 2.1\pi$, $\varphi_0 = 0.8\pi$; (P2- χ) $\varphi_{nl} = 1.7\pi$, $\varphi_0 = -0.9\pi$; (χ) $\varphi_{nl} = 2.5\pi$, $\varphi_0 = 0.2\pi$.

ceed to an investigation of temporal correlations. Figure 5 shows first return maps constructed from the same data as in Fig. 3. The return map labeled χ is an unstructured cloud around the bisector, whereas the P2 content of the data in P2- χ results in a splitting of the corre-

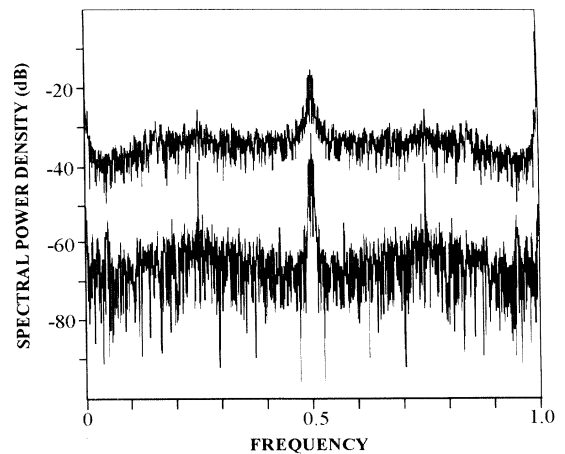


FIG. 4. Spectra showing the simultaneous occurrence of P4 and chaotic behavior at $\varphi_{nl} = 1.8\pi$, $\varphi_0 = 0.3\pi$. Top trace: square root of the second harmonic signal (PD2). Bottom trace: fundamental signal (PD3).

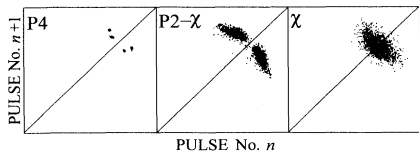


FIG. 5. Return maps (Lorenz plots) of the P4, P2- χ , and χ data displayed in Fig. 3. In all cases, the lower left corner is the origin (zero power).

sponding return map. These experimentally obtained maps look very different from the ones expected from a 1D map like Eq. (1). We will show below why this difference is indeed to be expected.

All results discussed up to this point were obtained with fiber B. From the discussion in Sec. II, we expect the amount of dispersion in the fiber to have a strong influence on the observed behavior. In particular, use of fiber A with its extremely small second order dispersion should bring us into a parameter regime in which the pulse formation in the cavity is strongly affected by third order dispersion β_3 , whereas with fiber C, only minor quantitative changes are expected.

Indeed, experiments with fiber C show essentially the same behavior as the ones discussed above, so that showing separate figures here seems unwarranted. However, with fiber A the length adjustment of the fiber ring is much more critical, and for deviations of more than a few tens or micrometers, much of the nonlinear behavior disappears. Even with the most careful adjustment of the cavity length, we find much less purely periodic behavior, and chaotic behavior covers a much wider section of the parameter range than before. Specifically, periodic evolutions are found in just a very small parameter range $\{-0.6\pi < \varphi_0 < 0, 0.3\pi < \varphi_{nl} < 0.6\pi\}$, and most of this is P2. It is hard to find P4, and we never saw higher periodicities than an occasional P16.

The experimental results presented so far already indicate by themselves that an explanation with a simple 1D map must fail just as much as a treatment of the pulses as entities that do not undergo internal changes. Instead, the observations can be naturally explained if pulse reshaping is taken into consideration. This is best addressed with a numerical simulation.

V. NUMERICS

We have implemented a numerical code to describe the combined action of dispersion and nonlinear optical mechanisms inside the fiber ring cavity. Our computation scheme basically consists of two steps for every round trip — propagation through the fiber and interference at the input coupler. Either step can be treated by conventional means. It is the combination of the two and their repetition that produce the phenomena described here. The propagation is described by a modified nonlinear Schrödinger equation [3]

$$\frac{\partial A(z, t)}{\partial z} + \frac{i}{2}\beta_2 \frac{\partial^2 A(z, t)}{\partial t^2} - \frac{1}{6}\beta_3 \frac{\partial^3 A(z, t)}{\partial t^3} = i\gamma |A(z, t)|^2 A(z, t), \quad (2)$$

with the optical amplitude A and the second and third order dispersion β_2 and β_3 , respectively. Linear losses in the fiber may be neglected here. We also explored inclusion of Raman scattering, but it turns out that for the parameter range discussed here it has no significant effect. This is in accord with experimental observations, and we will disregard Raman scattering in the following discussion.

Equation (1) is computed with the symmetrized split-step Fourier method [3]. We typically use a temporal discretization of $\Delta T = 50$ fs with a grid size of 1024 points and a spatial discretization Δz between 1 and 10 cm. Several conservation laws [16] are used to check the accuracy of the simulation. We find it important to optimize Δz and ΔT such that minimum deviations from the conservation of pulse energy $E = \int |A|^2 dt$ and of the quantity $\Phi = i \int (A \partial A^* / \partial t - \text{c.c.}) dt$ occur.

After every propagation there is interference with a new pulse from the light source. The complete n th round trip in the cavity can be calculated by the recurrence relation

$$A_n(0, t) = A_{in}(t) + \eta \exp(i\varphi_0) A_{n-1}(L, t). \quad (3)$$

We use a feedback efficiency $\eta = 0.41$, as calculated from the observed small signal finesse of the cavity. The simulation is initialized with zero power inside the cavity.

In comparison with Eq. (1) the variable A in this relation is now a function of space and time. There are in fact two time scales: “global time” is denoted by the round trip number n . “Local time” (time across the pulse) t and position z enter through Eq. (2). Also, A_{in} now represents the shape of the input pulses. Equations (2) and (3) therefore constitute a generalized version of Eq. (1).

Since the case of constant input power is contained in this extended model as a special case, we can reproduce the physical situation that is assumed in the Ikeda map by making $A_{in} = \text{const}$. Such a continuous wave simulation is not very realistic because competing processes like stimulated Brillouin scattering are not taken into account. Nevertheless, it can serve to give a first indication of at which power levels instabilities are to be expected. As anticipated, we find that the first bifurcation occurs when the maximum nonlinear phase, referred to a single fiber transit of the light, reaches the order of π . This is in accord with the results of Ikeda [1].

It is thus reasonable to expect that the far wings of the pulses, insofar as they have power less than this threshold, will not experience any dramatic modification by the nonlinearity. This reasoning is confirmed by the numerical results. Indeed, we find that only the central segment of the pulse, in which the power exceeds threshold, is affected strongly. A steep transition, much like a domain wall, forms in the wings close to the position where the power crosses threshold. We will therefore refer to the central part of the pulse, within the domain walls, as the nonlinear domain, and to the wings outside as the lin-

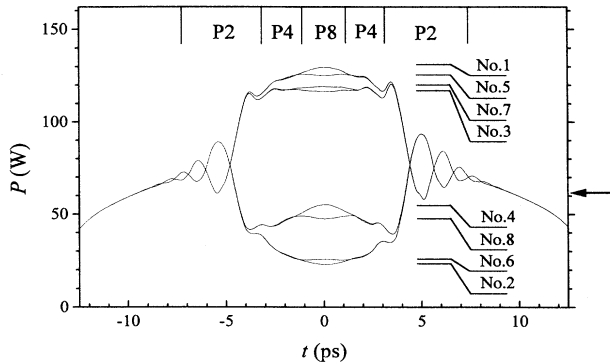


FIG. 6. Numerically simulated pulse profiles (power vs local time) of a period-8 evolution. $\varphi_{nl} = 1.1\pi$, $\varphi_0 = -0.45\pi$, $\beta_2 = 7.4 \text{ ps}^2/\text{km}$; $\beta_3 = -0.075 \text{ ps}^3/\text{km}$. Labels at top designate the dominant periodicity in the corresponding pulse region; labels on the side refer to the sequence of pulse profiles. The arrow indicates the threshold for the first appearance of a P2 in the iteration with constant input.

ear domain. Dispersion modifies the domain walls as the pulses propagate on.

Results of several runs of the simulation are shown in Figs. 6–10. In Fig. 6 the different stages of a P8 sequence are plotted into one graph. Clearly, zones of different periodic behavior are resolved. The region of P8 in the center of the pulse is surrounded by zones of decreasing period. The domain wall is located near the border between P4 and P2, and is indeed close to the point where the power exceeds the cw threshold. Undulations are created by the sudden jump of power at the domain wall

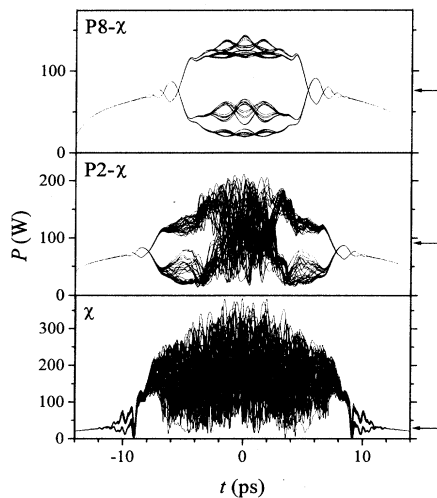


FIG. 7. Numerically simulated pulse profiles (power vs local time) in the chaotic regime. Each figure consists of 50 single traces. 800 preiterations served to let transients die out. P8- χ : $\varphi_{nl} = 1.2\pi$, $\varphi_0 = -0.45\pi$. P2- χ : $\varphi_{nl} = 1.7\pi$, $\varphi_0 = -0.5\pi$. χ : $\varphi_{nl} = 2.5\pi$, $\varphi_0 = 0.3\pi$. Dispersion: $\beta_2 = 7.4 \text{ ps}^2/\text{km}$; $\beta_3 = -0.075 \text{ ps}^3/\text{km}$ in all three examples. Arrows indicate the first appearance of a P2 in the iteration with constant input.

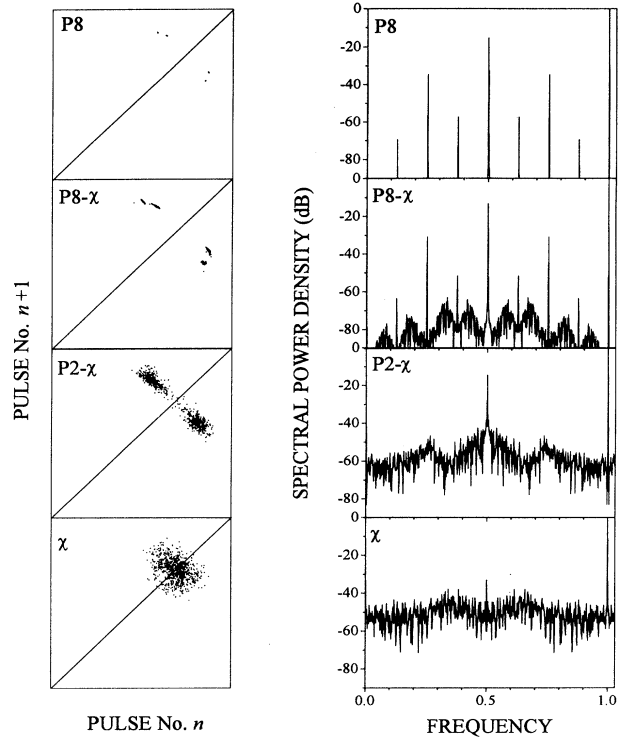


FIG. 8. Return maps and spectra of the time series corresponding to the spatial pulse structures displayed in Figs. 6 and 7. 500 preiterations served to let transients die out. In all return maps, the lower left corner is the origin (zero power). Note that this figure shows signals as they would appear at detector PD3 while all other computational results shown in this paper are referred to the entrance face of the fiber.

and move out into the linear domain where they seem to decay exponentially. They change phase every round trip and thus form a P2 regime.

An example for simultaneous occurrence of periodic and chaotic behavior is shown in Fig. 7 (panel P8- χ). Here, the same resonator phase was assumed as in Fig. 6,

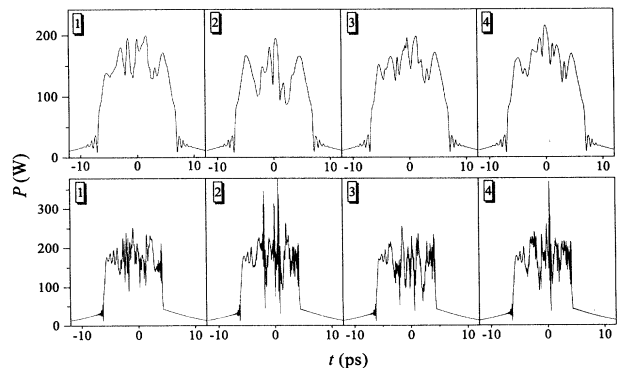


FIG. 9. Simulation of four subsequent pulse shapes in the chaotic regime for different dispersion. $\varphi_{nl} = 1.4\pi$, $\varphi_0 = 0.65\pi$. Top panels: $\beta_2 = 7.4 \text{ ps}^2/\text{km}$, $\beta_3 = -0.075 \text{ ps}^3/\text{km}$; bottom panels: $\beta_2 = 0.5 \text{ ps}^2/\text{km}$, $\beta_3 = -0.08 \text{ ps}^3/\text{km}$.

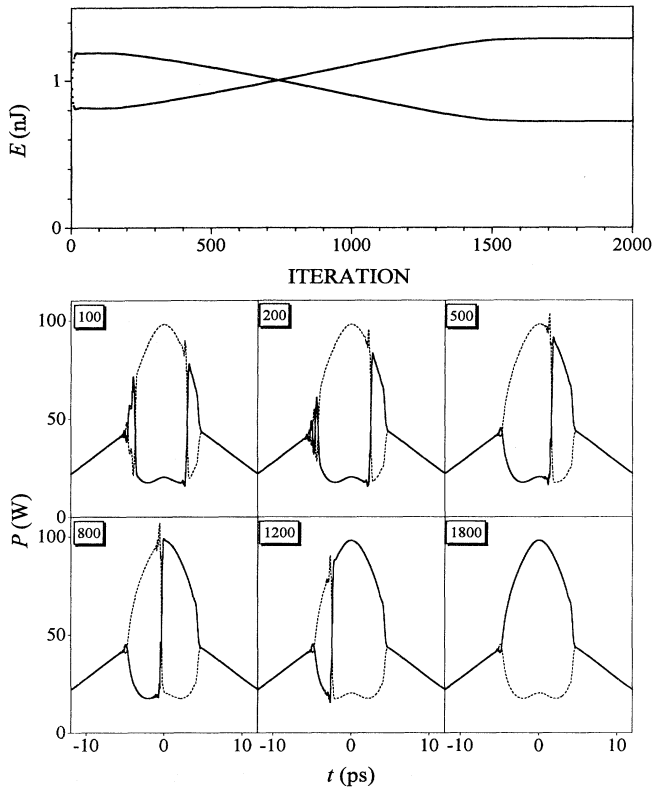


FIG. 10. Numerical simulation of the transient behavior of pulse profiles leading to the “wiggly” bifurcation. $\varphi_{nl} = \pi$, $\varphi_0 = 0.05\pi$, dispersion as in Fig. 2. Top trace: Evolution of pulse energy vs global time. Bottom panels: Solid lines refer to the pulse profile at the displayed iteration number; dashed lines show the pulse profile after one more iteration step.

but the input power was raised slightly. Again, there are domain walls close to the cw threshold, and the P2 regime looks very similar to the previous case. The periodic zones up to P8 already appear fuzzy, and there is chaotic dynamics in the pulse center. Upon further increase of input power the fuzziness increases to the point where little (Fig. 7, panel P2- χ) or no (panel χ) indication of periodic behavior is present in the nonlinear domain. Note that the last two graphs have been calculated for parameters similar to those pertaining to the experimental observation of the return maps and spectra in Figs. 3 and 5.

Figure 8 shows the power spectra and return maps pertaining to the data of Figs. 6 and 7. A comparison with the experimental spectra and return maps in Fig. 4 reveals detailed agreement. In particular, the return maps in the chaotic regime are washed out in a similar way. This is, of course, a result of the more or less independent temporal evolution of different segments of the pulse.

The influence of dispersion is best demonstrated under conditions of fully developed chaos, i.e., chaos with almost no periodic content. Two short numerical sequences of chaotic pulse profiles are displayed in Fig. 9. All parameters are equal, except dispersion. The top-hat-like

pulse shapes make the distinction between the central nonlinear domain and the linear domain in the slopes very clear. Both examples show fragmentation in the nonlinear domain, and in either case, the domain walls are close to the cw threshold and seem to seed undulations.

On the other hand, there are also obvious differences: The substructures are relatively smooth in the case of high dispersion, and much more spiky for low dispersion. In the latter case, third order dispersion makes itself noticeable through an obvious asymmetry in the pulse profiles: The undulations are visible only in the trailing slope, and the spikiness is most severe in the leading half of the nonlinear domain.

This asymmetry due to third order dispersion is also responsible for the “wiggly” behavior in the transients mentioned in the section on experimental results. The top panel of Fig. 10 shows an example of the transient evolution of pulse energies in a P2 regime. The panels below show the pertaining pulse shapes at different stages in that evolution. In each panel, two traces are shown: the solid line refers to the iteration step as given in the label; the dashed line shows the next pulse. Both subsequent pulses are almost indistinguishable in the linear domain. In contrast, inside the nonlinear domain the subsequent pulse seems to be a flipped-over version of the previous one. This leads to an alternation in pulse energy: Pulses at even iteration numbers (solid line) have lower energy, and at odd numbers the energy is higher. This change in pulse energy would manifest itself as a P2 behavior in an experiment.

Again, the steep domain walls seed undulations, which are more apparent in the trailing slope. At the leading domain wall, a shock front begins to move into the nonlinear domain at an early stage (iteration number 100) and continues to walk across the pulse.

After about 800 iterations the shock front has reached center pulse. Here, flipping over does almost nothing to the pulse energy. As the front moves on, there is again an alternation between two pulse energies. Note, however, that now *even* pulses have higher energy. Thus a crossover in the pulse energy pattern has occurred. In this example there is only one shock front, and thus a single crossover. Multiple shock fronts will lead to “wiggly” bifurcations as observed in the experiment.

We therefore explain the wiggles as a transient phenomenon in the presence of third order dispersion. Note that for the parameters used in Fig. 10 β_2 is the dominant order of dispersion on time scales down to $\tau = |\beta_3/\beta_2| \approx 10$ fs [3]. This makes it clear why the wiggles occur more pronouncedly in the case of fiber A with its extremely low second order dispersion and therefore more prominent third order dispersion (in that fiber, third order dispersion takes over for structures shorter than ≈ 160 fs).

The explanation holds even semiquantitatively: the propagation speed relative to the pulse, 5 fs per round trip in this example, turns out numerically to be proportional to β_3 , both in amount and sign. In fact, we never observed “wiggles” and the propagation of shock fronts in the pulse in the case of $\beta_3 = 0$. Note, however, that this situation cannot be accessed experimentally, as there

is always a contribution of higher order dispersion. Also, the speed of propagation roughly corresponds to the difference in propagation delay for two Fourier components that are spread out in frequency by the inverse of the rise time of the shock front, 300 fs.

Both the shock fronts in the “wiggly” bifurcation and the spatial undulations in the pulse profiles are closely related phenomena. In the absence of dispersion we observe the formation of a discontinuity at the domain wall (compare [5]). Due to dispersive coupling this discontinuity is not only washed out but rather leads to the formation of shock fronts and oscillatory structures.

VI. DISCUSSION

The experimentally recorded time series can represent each pulse only by one number — its energy. Nevertheless, we provided ample evidence that the shapes of the individual pulses are subject to dramatic changes. Pulse substructure is being formed that may be stationary, or evolve periodically or even chaotically. A number of more or less indirect clues were obtained from the experiment, and a numerical analysis was able to explain all observations. Thus we arrive at a detailed picture of the spatiotemporal structure formation.

The fact that the pulse energies undergo period-doubling bifurcations has been observed by other authors before [2,5,6], if not with the same clarity as achieved here. The signal-to-noise ratio of our experiment allows detection of P32; also, the important parameter of resonator phase is measured so that meaningful comparisons with theory are feasible.

In addition to showing this temporal bifurcation scheme, our combination of experimental and numerical results provides a clear indication that there also is a spatial instability coupled to the temporal instability. This instability can be followed through the subharmonic and into the aperiodic regime. In the latter, we deal with turbulence, i.e., spatiotemporal chaos. The key parameter to couple spatial and temporal structures is dispersion. Dispersion, which has been disregarded in some of the early investigations, was systematically varied in this work.

All our observations can be well understood in the picture of pulses composed of small temporal slices. Assuming precise cavity length adjustment for exact synchronism with the pump pulse train, each slice interacts with its corresponding slice in the subsequent pulse through interference once every round trip. In the absence of dispersion (a very artificial assumption), there would be no coupling between neighboring slices. One would then have to consider infinitesimally narrow slices, and thus arrive at the paradox mentioned in the Introduction.

Dispersion will, of course, introduce coupling between neighboring slices [9]. In other words, while interference provides an interaction in “global time,” dispersion does so in “local time.” For finite dispersion, it is therefore more reasonable to consider slices of some finite width that scales with the amount of dispersion present: The less dispersion, the shorter the correlation in local time.

In a comoving frame of reference, structure in local time translates into spatial structure. We conclude that the interplay of Kerr nonlinearity, dispersion, and repetitive interference forms longitudinal spatial substructure in the pulses.

The pulses used in our experiments are between one and two orders of magnitude wider than the typical size of the substructures in the pulse (Figs. 7 and 9). The effective number of degrees of freedom is therefore high. Due to this high number of degrees of freedom, return maps in the chaotic parameter range are smeared out to the unstructured clouds as displayed in Fig. 8. For the same reason, it is difficult in the case of the low dispersion fiber to find parameters where all of the pulse undergoes periodic evolution; most of the time some part of the pulse evolves chaotically, so that the recorded time series which average over all of the pulse will rarely show purely periodic dynamics.

Of course, any misalignment of the ring cavity length from precise synchronism with the input pulse train will introduce an additional interaction between otherwise independent slices (see also [17]). It is therefore clear why length adjustment is more critical with less dispersion, as was found experimentally. Note that length misalignment creates a coupling that acts in one direction. It therefore more closely resembles the effect of third order dispersion, since second order dispersion acts symmetrically.

Since we can record time series long enough for meaningful evaluation with statistical methods, we are able to calculate quantitative information about the degree of complexity in the problem. Such detailed time series analysis will be presented in a forthcoming paper.

VII. OUTLOOK

The synchronously driven resonator is closely related to a famous standard example of a chaotic system, the kicked rotator [18]. The main difference is that here the duration of the “kick” is not arbitrarily short: It is much longer than the shortest time constant in the system, the optical cycle. Therefore, and because of the wave nature of optical fields, we have to discuss *interference* once every round trip.

We have shown that spontaneous formation of structures evolves from this self-interference. In contrast to most work on pattern formation in nonlinear optics, we deal here with a longitudinal structure. While this is technically more difficult to study in an experiment, it is interesting in that we have a truly one-dimensional spatial system. It should therefore be more traceable by mathematical techniques, e.g., coupled maps, and provides an intermediate step in the understanding of the even higher complexity of turbulence in all spatial dimensions.

The coupling length, and thus the effective number of degrees of freedom, can be chosen at will in our system. In contrast, it is generally hard in other systems to vary

the aspect ratio, or Fresnel number, over a large range without changing other parameters — let alone change the sign.

In fact, by variation of fiber dispersion one should be able to scan the whole transition range from purely temporal, i.e., low-dimensional chaos to full spatiotemporal turbulence. Our numerical simulations provide guidance in designing such an experiment. It might also be interesting to perform a similar experiment as described here in the regime of anomalous dispersion where optical solitons can be expected to form. Such experiments are now underway.

Let us finally point out that a better understanding of this system might pave the way to an enhanced understanding of mode-locked lasers, which are the “active” counterpart of the passive resonator considered here. For example, our experiment bears striking similarities with an additive pulse mode-locked laser, in which a synchronously driven resonator containing a fiber is responsible for the shaping of short light pulses. In our opinion

it is not unusual that chaotic processes are at work in such lasers. However, this fact goes unnoticed most of the time, and very few reports are available today that point it out [19]. We hope that it will become more widely appreciated in the future.

ACKNOWLEDGMENTS

We thank Tektronix for the loan of the RTD710A digital oscilloscope and LeCroy for the loan of the model 9354L. We also thank Dr. C. Emslie of Fibercore for helping us to select the fibers used here. It is a pleasure to acknowledge interesting discussions with J. Herrmann und S. Gatz, who also gave helpful advice about the numerical procedure. The numerical calculations reported here were made possible by the computer workstation pool of the physics department at the University of Hannover. Financial support from Deutsche Forschungsgemeinschaft is gratefully acknowledged.

-
- [1] K. Ikeda, *Opt. Commun.* **30**, 257 (1979); *J. Phys. (Paris) Colloq.* **44**, C2-183 (1983); K. Ikeda, H. Daido, and O. Akimoto, *Phys. Rev. Lett.* **45**, 709 (1980); K. Ikeda, K. Kondo, and O. Akimoto, *ibid.* **49**, 1467 (1982).
 - [2] H. Nakatsuka, S. Asaka, H. Itoh, K. Ikeda, and M. Mat-suoka, *Phys. Rev. Lett.* **50**, 109 (1983).
 - [3] G. P. Agrawal, *Nonlinear Fiber Optics* (Academic Press, Boston, 1989), pp. 19, 43–48, 101.
 - [4] J. V. Moloney, in *Instabilities and Chaos in Quantum Optics II*, edited by N. B. Abraham, F. T. Arecchi, and L. A. Lugiato (Plenum, New York, 1988), pp. 193–218.
 - [5] R. Vallée, *Opt. Commun.* **81**, 419 (1991).
 - [6] M. B. van der Mark, J. M. Schins, and A. Lagendijk, *Opt. Commun.* **98**, 120 (1993).
 - [7] M. Nakazawa, K. Suzuki, and H. A. Haus, *Phys. Rev. A* **38**, 5193 (1988).
 - [8] M. Haeltermann, S. Trillo, and S. Wabnitz, *Opt. Commun.* **91**, 401 (1992).
 - [9] R. Vallée, *Opt. Commun.* **93**, 389 (1992).
 - [10] G. Steinmeyer, D. Jaspert, and F. Mitschke, *Opt. Commun.* **104**, 379 (1994).
 - [11] F. Mitschke, G. Steinmeyer, A. Buchholz, and M. Hänsel, in *Proceedings of the Second Experimental Chaos Conference*, edited by W. L. Ditto, L. Pecora, M. L. Spano, M. Shlesinger, and S. T. Vohra (World Scientific, Singapore, in press).
 - [12] D. W. McLaughlin, J. V. Moloney, and A. C. Newell, *Phys. Rev. Lett.* **54**, 681 (1985).
 - [13] F. Mitschke, G. Steinmeyer, M. Ostermeyer, C. Fallnich, and H. Welling, *Appl. Phys. B* **56**, 335 (1993).
 - [14] J. Vobian, *J. Opt. Commun.* **11**, 29 (1990).
 - [15] R. H. Stolen and C. Lin, *Phys. Rev. A* **17**, 1448 (1978).
 - [16] S. Gatz and J. Herrmann, *IEEE J. Quantum Electron.* **QE-28**, 1732 (1992).
 - [17] S. Gatz and J. Herrmann, *Opt. Commun.* **104**, 405 (1993).
 - [18] H. G. Schuster, *Deterministic Chaos* (Physik-Verlag, Weinheim, 1984), p. 12.
 - [19] G. Sucha, S. R. Bolton, S. Weiss, and D. S. Chemla, in *Conference on Lasers and Electro-Optics*, OSA Technical Digest Series (OSA, Washington, DC, 1993), Vol. 11, p. 146.